Light Metals 2011 *Edited by: Stephen J. Lindsay*
TMS (The Minerals, Metals & Materials Society), 2011

Light Metals 2011

ELECTRODE TECHNLOGY for ALUMINUM PRODUCTION

Inert Anodes and Wettable Cathodes

SESSION CHAIR
Veronique Laurent
Rio Tinto Alcan
Voreppe Cedex, France

Jilai Xue
University of Science and Technology
Beijing, China

Light Metals 2011 *Edited by: Stephen J. Lindsay*
TMS (The Minerals, Metals & Materials Society), 2011

PRESSURELESS SINTERING OF TIB2–BASED COMPOSITES USING TI AND FE ADDITIVES FOR DEVELOPMENT OF WETTABLE CATHODES

Hamed Heidari[1]; Houshang Alamdari[1]; Dominique Dubé[1]; Robert Schulz[2]

[1] Department of Mining, Metallurgical and Materials Engineering, Université Laval, Québec (QC), Canada G1V 0A6
[2] Hydro-Quebec Research Institute, 1800 Boul. Lionel Boulet, Varennes, QC, Canada J3X 1S1

Keywords: Pressureless liquid phase sintering, Wettable cathode, Titanium diboride (TiB_2) composite.

Abstract

Titanium diboride is the most promising candidate material for development of wettable cathodes for aluminum smelting. It is considered as an alternative for carbon cathodes in order to reduce the anode cathode distance resulting in higher energy efficiency in electrolysis cells. In this work, TiB_2-based ceramic specimens were consolidated using metallic additives followed by pressureless sintering. Different proportions of iron and titanium ($\leq$ 10 wt%) were used as low melting point sintering additives. Sintering was conducted at 1400–1650°C under controlled atmosphere. The effects of composition, sintering temperature, milling time and pre-alloying of the additives on densification, microstructure, and mechanical properties were investigated. It was found that pre-alloying and milling time have significant influence on densification, microstructure uniformity and bending strength. Uniform crack-free microstructure with even distribution of pores as well as maximum relative density of 91% and bending strength of 300 MPa were obtained using pre-alloyed additives, milling time of 30 min and sintering for 1 h at 1650°C.

Introduction

Liquid aluminum reacts with almost all materials with only a few having good stability [1]. Most of the stable materials are very expensive metals or non conductive ceramics, which are major obstacles for their application as cathode material. Nevertheless there are some electrically conductive ceramics such as graphite and TiB_2. Graphite has been used for more than a century in aluminum electrolysis cells [2]. However, liquid aluminum does not wet graphite. Thus a relatively thick liquid metal pad is kept on top of the graphite cathode to avoid the diffusion of electrolytes through the cathode blocks and to insure good electrical current distribution within the cell. The magnetic fields present in smelting cells apply significant Lorentz forces on the metal pad resulting in wave creation. In order to avoid the short circuits between the metal pad and anode, the anode-cathode distance is kept large (typically 4.5 cm) unnecessarily increasing the bath resistance [3, 4].

TiB_2 has very high melting point (about 3000°C), low density, excellent strength, high hardness, and very good thermal and electrical conductivities [5-7]. It is chemically stable in and well wetted by liquid aluminum [3, 4, 8]. It has been therefore the most promising in the attempts to find an alternative material for carbon cathodes since the search began in the 1950's [9]. Despite its extraordinary properties, strong covalent bonding and low diffusion coefficient make sintering of TiB_2-based ceramics quite difficult [7].

Fully dense TiB_2 is probably not necessary for cathode application. It has been shown that using dense TiB_2 cathodes results in early failure by cracking [10]. Liquid aluminum reacts with impurities at grain boundaries and, after a period of time, results in the formation of new phases, internal stress build up and crack formation [11].

A number of techniques have been used to consolidate TiB_2 [12-15]. Pressureless sintering is a low cost technique to produce large and near net-shape components. However to consolidate pure TiB_2 with this technique, very high sintering temperatures are required resulting in exaggerated grain growth and reduced mechanical properties. It has been reported that at temperatures above 1700°C, the presence of titanium oxide at the surface of particles increases both pore and grain size by increasing the surface diffusivity [16, 17]. In industrial conditions, it is difficult to remove this oxide layer. Thus, it is preferred to sinter TiB_2-based ceramics below 1700°C. At these relatively low temperatures the use of sintering additives are almost unavoidable to provide a liquid phase promoting consolidation of TiB_2-based composite. Under these conditions, the sintering of TiB_2-based composite requires an appreciable amount of liquid phase, wettability of TiB_2 by the liquid phase, and small solubility of the solid phase in the liquid [18].

In this study, titanium and iron were used as additives to reduce the sintering temperature. Titanium was chosen as the principal metallic additive. Upon infiltration of aluminum into the porous cathode, it could react with the titanium additive to produce $TiAl_3$ with a melting point higher than that of aluminum. $TiAl_3$ also shows a very good wettability with respect to molten aluminum. Although $TiAl_3$ is soluble in liquid Aluminum, it has been shown to be stable when formed at the surface of TiB_2 [19, 20]. Iron, in turn, was chosen to somewhat reduce the melting point of additives. Ti and Fe have a eutectic at 1078°C and 71.1 mol% Ti [21]. These metals wet the surface of TiB_2 [22] while TiB_2 has a small solubility in liquid Ti-Fe [23].

The TiB_2-Fe system is characterized also by a eutectic at 1340°C and 6.3 mol% TiB_2 [24]. The reaction between TiB_2 and Fe may accelerate densification and lead to the formation of Fe_2B. This phase could cause deterioration in the mechanical properties as well as the resistance to liquid aluminum. The presence of titanium in the liquid mixture could prevent the formation of Fe_2B [25]. Fe can also react with liquid aluminum to form $FeAl_3$ having a melting at about 1160°C [26].

In this work, the effects of different compositions, processing conditions, and sintering temperature on density, microstructure and mechanical properties were investigated. A total amount of 10 wt% Ti and Fe was selected as metallic additives to provide about 10 vol% of liquid phase during sintering.

Materials and methods

Commercial TiB_2, Ti and Fe powders (Atlantic Equipment Engineers Inc., Bergenfield, NJ) were used as starting materials. The particle size of TiB_2 powder was between 2 and 10 μm with a mean size of 6 μm. Its purity was >99.7 % and the impurities were

C, N, O and Al. For Ti powder the particle size was <20 μm and for Fe powder, the particle size was between 1 and 9 μm.

The TiB_2 powder was mixed with selected proportions of Ti and Fe powders and then milled in a high energy ball mill (SPEX 8000, Spex Industries, Inc., Edison, NJ) using hardened steel vial and balls with a ball-to-powder weight ratio of 4:1. Ti and Fe powders were added to TiB_2 either separately or after being pre-alloyed.

Pre-alloying of Ti and Fe powders was performed, first by mixing titanium and iron in a 70:30 Ti:Fe weight ratio and then by pressing the powder mixture at 400 MPa using an uniaxial steel die. The compacted specimens were then sintered at 1150°C for 1 hour. The resulting pellets were subsequently crushed and milled using high energy ball milling for 1 h to obtain the pre-alloyed additive in powder form. XRD analysis showed the presence of α-Ti and the FeTi intermetallic compound in this powder.

The TiB_2-Ti-Fe powder mixtures were pressed at 150 MPa in a uniaxial die to form pellets of 16 mm in diameter and bars of 38 × 13 mm. The specimens were then heated in a tube furnace (INP15-20, Norax Canada inc., QC) at a rate of 6°C/min from room temperature to the specified sintering temperature. Sintering of pellets was performed under an Ar/5%H_2 protective atmosphere for 1 hour. The various experimental conditions of this study are given in Table I.

Table I- Experimental conditions used for consolidation of specimens

No.	Code*	Additives wt%** Ti	Fe	Sintering Temperature (°C)	Pre-alloying	Milling time (min)
1	T8F2M10	8	2	1400-1600-1650	-	10
2	T7F3M10	7	3	1400-1600-1650	-	10
3	T8F2M30	8	2	1650	-	30
4	T7F3PM10	7	3	1600-1650	yes	10
5	T7F3PM30	7	3	1650	yes	30
6	T7F3PM60	7	3	1650	yes	60
7	T7F3PM120	7	3	1650	yes	120
8	T7F3PM240	7	3	1650	yes	240

**T: Titanium, F: Iron, P : Pre-alloying, M : milling time*

***Unless noted, all compositions in this article are in weight percent*

The green density of specimens was evaluated by measuring their weight and geometrical dimensions. The bulk density of sintered specimens was determined using the Archimedes method with isopropanol as the immersing medium. Theoretical density was estimated using the rule-of-mixtures calculations that assumed the nominal compositions of the powder specimens as specified. Relative densities were calculated by dividing the measured bulk density by the calculated theoretical density. Based on replicated measurements on identical specimens, the uncertainty on relative density was estimated to be less than ±1%. Hence, no error bar was included in the figures.

The bending strength of the sintered specimens was measured using the three-point bending test with a 26 mm span at a loading rate of 0.5 mm/min according to the ASTM C1161 standard [27]. The dimensions of the test specimens used for bending strength measurements were 38 mm × 13 mm × 4 mm.

For microstructural investigations, the specimens were cut with a diamond saw and polished to 0.1 μm surface finish using successively finer diamond abrasives. The microstructure of specimens was investigated using a scanning electron microscope and the chemical microanalysis was performed by energy dispersive X-ray spectroscopy (EDX; *PGT Avalon*, Princeton, NJ). The crystalline structure was determined by X-ray diffraction method (XRD; Siemens D5000) with a Cu K_α radiation at a scanning rate of 1° min^{-1}.

Wettability of sintered specimens was studied by placing a 90 mg aluminum piece at the surface of sintered specimen surface and heating under high vacuum ($1.2E^{-5}$ mbar) to 960°C. The wetting angle was monitored using an instant imaging system. From these images, contact angles can be measured as a function of time.

Results and discussion

Effect of additive composition

The relative density was measured for specimens with two different compositions after sintering at 1400, 1600 and 1650°C. As shown in Figure 1, at all sintering temperatures, specimens containing 7wt% Ti and 3% Fe (T7F3M10) had higher density than that of specimens containing 8% Ti and 2% Fe (T8F2M10). According to the Fe-Ti phase diagram [28] the additive with a mass ratio of 7Ti:3Fe is closer to eutectic. A lower melting point leads to earlier formation of liquid phase during sintering, therefore promoting better densification.

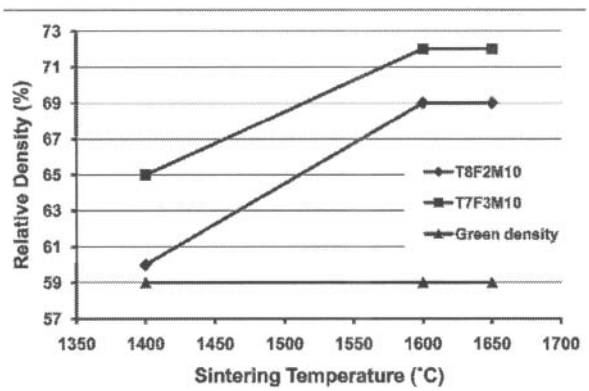

Figure 1- Comparison of the relative density as a function of sintering temperature and composition of sintering additives (T8F2M10: TiB_2+8%Ti+2%Fe; T7F3M10: TiB_2+7%Ti+3%Fe).

Effect of sintering temperature

As shown in Figure 1, for both compositions (T7F3M10 and T8F2M10), there is not much densification after sintering at 1400°C. However, sintering at 1600 and 1650°C resulted in an appreciable densification to approximately 70%. Between 1600 and 1650°C, there is no further densification. An SEM backscattered (BS) micrograph of the T8F2M10 specimen, sintered at 1400°C, is presented in Figure 2. It shows that the additives formed segregated phases. A temperature of 1400°C, well below the melting point of Fe and Ti, is not high enough to provide the liquid phase required to promote densification. Moreover, these additives were not locally mixed in the proper ratio and were not in intimate contact with each other.

When Fe and Ti particles are in intimate contact, solid state diffusion occurs at the interface resulting in the formation of a thin liquid layer in between. Increasing the sintering temperature to 1600°C resulted in the formation of significant amount of liquid and consequently in higher densification of specimens.

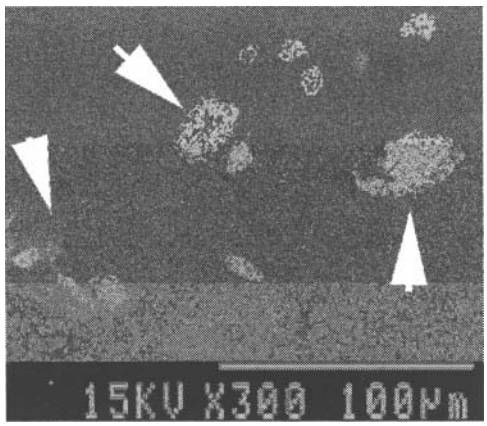

Figure 2- Backscattered SEM micrograph of T8F2M10 (TiB_2+8%Ti+2%Fe) specimen, sintered at 1400°C for 1 h (The arrows show segregated phases containing the additives).

Effect of pre-alloying additives

Besides the uniform distribution of additives, it is important to have Ti and Fe particles in contact with each other to promote the formation of the liquid phase. Hence, the addition of pre-alloyed additives, instead of adding Ti and Fe separately, was considered to achieve this goal. The pre-alloyed additives were prepared by mixing, pressing, and sintering Ti and Fe powders with a mass ratio of 7:3.

Table II compares the relative densities of specimens with pre-alloyed additives (T7F3PM10) with those obtained by adding the additives separately (T7F3M10) after sintering at two different temperatures. Under the same processing and sintering conditions, pre-alloying of the additives resulted in better densification. The difference is significant at 1650°C.

Table II- Relative density of specimens with separate (T7F3M10) and pre-alloyed (T7F3PM10) additives

Specimen	Relative density (%)		
	Green Density	Sinter. 1600°C	Sinter. 1650°C
T7F3M10	59	72	72
T7F3PM10	62	74	80

Effect of milling time

Milling was performed in order to achieve a uniform distribution of additives. However, milling time should be as short as possible to reduce costs and to prevent oxidation of powders. To investigate the effect of milling time on the densification process, powder mixtures were milled for different times prior to sintering. Preliminary results showed that by increasing the milling time from 10 to 30 min, density after sintering increased. These preliminary experiments suggest that the milling time has an important influence on densification. The effect of milling time was further investigated in a systematic way for specimens containing 90 wt% TiB_2 , 7 wt% Ti, and 3 wt% Fe using five different milling times (10, 30, 60, 120 and 240 minutes) followed by compaction and sintering at 1650°C. (Specimens 4-8, Table I). The densities of specimens (green and after sintering) were plotted as a function of milling time in Figure 3. No significant influence of milling time on green density was observed. However specimens milled for 30 min showed a maximum density of 91% after sintering. Further milling resulted in a slight decrease in density. Figure 4 shows that the three-point bending strength of sintered specimens follows a similar trend: a maximum bending strength of 300 MPa was achieved for specimens milled 30 min.

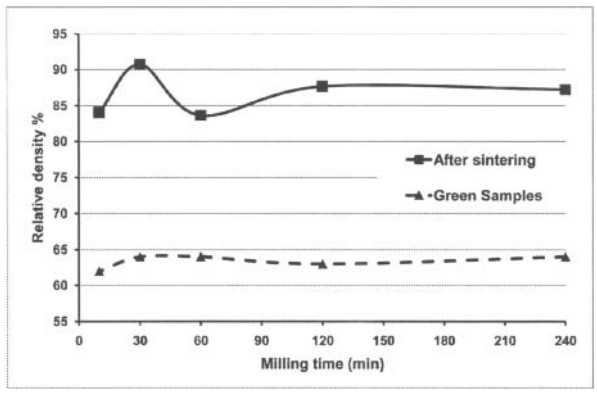

Figure 3- Influence of milling time on relative density of green and sintered specimens (TiB_2+7%Ti+3%Fe) using pre-alloyed additive and sintered at 1650°C for 1h.

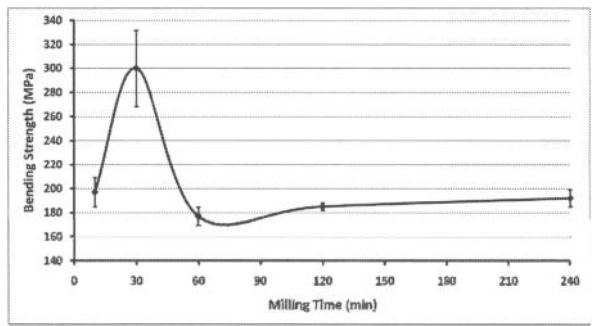

Figure 4- Influence of milling time on bending strength of specimens (TiB_2+7%Ti+3%Fe) prepared using pre-alloyed additive and sintered at 1650°C for 1h.

In order to understand the influence of milling time on sintering, the particle size distribution was determined and XRD analyses were performed on milled powders while the microstructure of sintered specimens was investigated by SEM.

The effect of milling time on the particle size distribution of powders is shown in Figure 5. After 10 min of milling, the powder mixture is mainly composed of particles with a mean size of 6 micrometers similar to that of the starting TiB_2 powder. However, a wider particle size distribution was observed. This distribution widening as well as the appearance of a shoulder at around 2 micrometers is most likely due to the TiB_2 particle fracturing and refining during milling. In addition, EDX analysis of the very large particles showed that the peak at 200 micrometers is related to the Ti and Fe pre-alloyed particles. Milling of mixed powders for 10 min reduced the particle size of additive powders, but some large additive particles remained. Milling for 30 min, however resulted in a quite different particle size distribution. The distribution is much wider and shifted toward the small diameters. The quantity of particles smaller than 0.7 micrometer increased, and the peak related to the metallic additive particles disappeared. This suggests that milling for 30 minutes results in a good refining and dispersion of metallic additives within the powder mixture

and provides partial refining of TiB_2 particles (particles smaller than 0.7 micrometer).

By increasing the milling time to 60 min, a second peak appeared in the particle size distribution at around 100 micrometers. Since the powder samples are deagglomerated using an ultrasonic bath prior to analysis, the presence of this second peak suggests the formation of strong agglomerates in the powder. By further increasing the milling time, the quantity of these strong agglomerates increases but no significant increase is observed in the quantity of small particles. EDX analysis of large agglomerates showed that they were rich in Ti and Fe. They are usually formed by plastic deformation and cold welding of smaller particles and are very difficult to deagglomerate even in an ultrasonic bath.

The typical shape of the large agglomerates observed after 240 min of milling is shown in Figure 6. These large particles are basically composed of TiB_2 particles welded together by metallic additives.

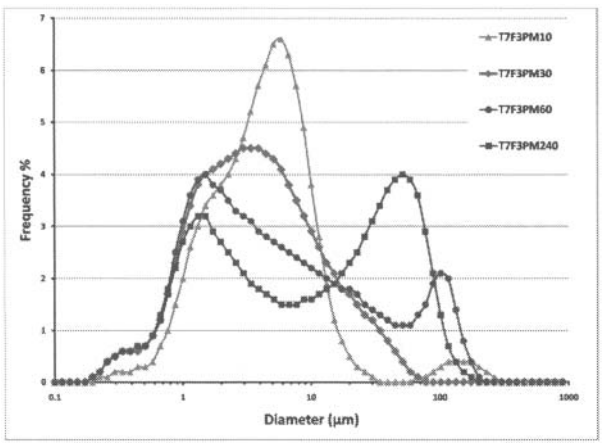

Figure 5- Effect of milling time on the particle size distribution for powder mixtures containing the 70%Ti and 30%Fe pre-alloyed additive.

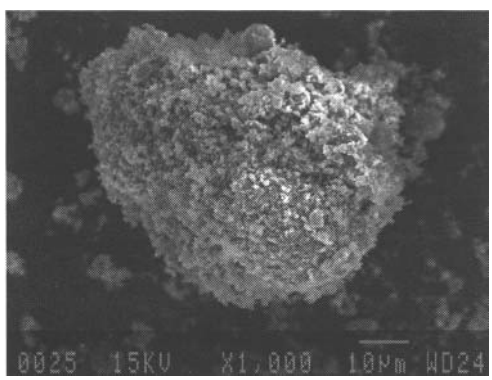

Figure 6- SEM micrograph of a large agglomerate formed after 240 min milling in T7F3PM240 powder (TiB_2+7%Ti+3%Fe).

The XRD patterns of the TiB_2 powders milled for 10 and 240 min are shown in Figure 7. The peaks were slightly broadened after 240 min of milling while the intensities decreased owing to the overall decrease of the crystal size of TiB_2. At the resolution of these x-ray scans, the minor phases corresponding to the pre-alloyed additives were not detected.

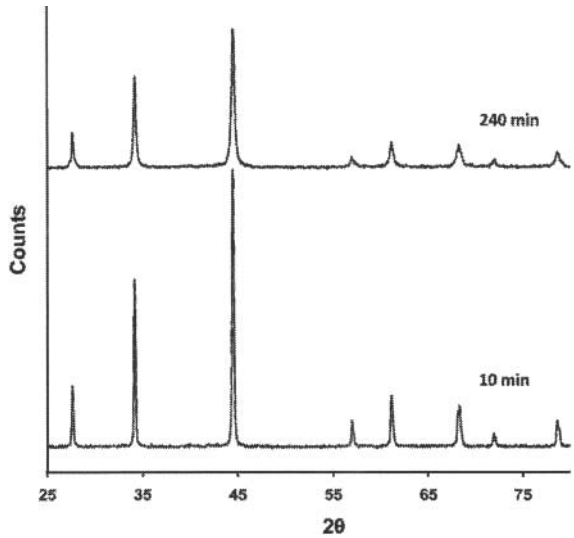

Figure 7- XRD analysis of powders containing pre-alloyed additives after 10 and 240 min milling. (Cu Kα).

SEM micrographs of polished sections of specimens containing pre-alloyed additives and sintered at 1650°C are shown in Figure 8 to Figure 10. In Figure 8, the microstructure of the specimen milled for 10 min revealed a highly porous structure. The high level of porosity explains the low density (84%) and reduced bending strength of this specimen (197 MPa). By increasing the milling time to 30 min (Figure 9), a more uniform and denser microstructure was achieved after sintering. A significant increase of density (91%, Figure 3) and bending strength (300 MPa, Figure 4) was observed for this specimen compared with the previous one.

As shown in Figure 5, after 30 min of milling, there was a refinement of the particle size and a broader distribution was observed leading to higher densification. During liquid phase sintering, densification is mostly caused by rearrangement of particles upon formation of the liquid phase [29]. Further densification is achieved by the solution-precipitation process: small particles promote this stage due to their higher surface energy and therefore higher solubility in the liquid phase [29]. A broader particle size distribution increases the overall contact area between particles and eases the particle rearrangement in the early stage of sintering. Moreover, the presence of small particles can help the solution-precipitation stage. As a result, higher densification and bending strength could be achieved after 30 min of milling.

By further increasing milling time, densification and bending strength decrease. As revealed by the microstructure of T7F3PM120 specimens ball milled for 120 min (Figure 10), cracks were formed after sintering. These cracks explain the dramatic decrease of bending strength (Figure 4). Crack formation was attributed to the presence of hard agglomerates in the powder mixture. As shown in Figure 6, these large agglomerates are formed by the cold welding of TiB_2 particles with additive particles. In the early stage of milling, the TiB_2 particles are partially refined and stick to the additives. Upon further milling, the TiB_2 particles become embedded in additives and form large and dense agglomerates. Upon sintering, these large agglomerates shrink initiating cracks around them in the compact. This phenomenon has also been reported previously [18, 29]. These

cracks limit the densification of the sintered specimens and reduce their strength.

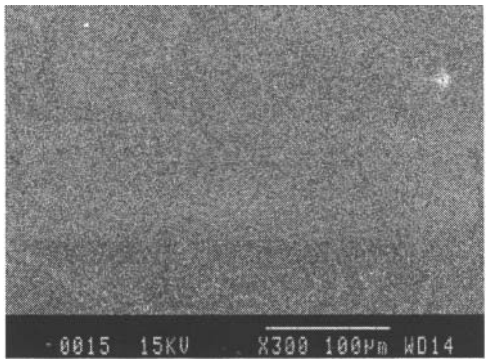

Figure 8- Backscattered SEM micrograph of T7F3PM10 specimen (TiB_2+7%Ti+3%Fe) milled for 10 min and sintered 1 h at 1650°C.

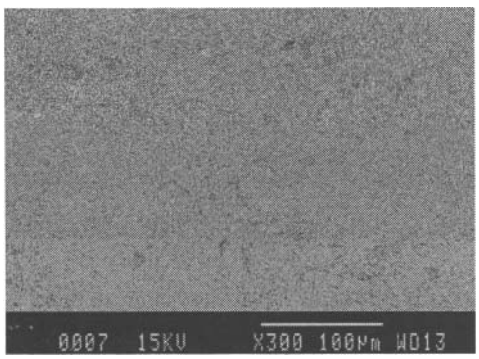

Figure 9- Backscattered SEM micrograph of T7F3PM30 specimen (TiB_2+7%Ti+3%Fe) milled for 30 min and sintered 1h at 1650°C.

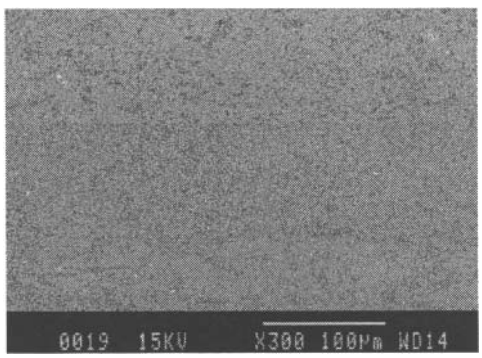

Figure 10- Backscattered SEM micrograph of T7F3PM120 specimen (TiB_2+7%Ti+3%Fe) milled for 120 min and sintered 1 h at 1650°C.

Wettability and stability in liquid aluminum

Since specimens milled 30 min with pre-alloyed additives (T7F3PM30) show the best density, strength and uniform microstructure, their wettability by liquid aluminum was investigated. Figure 11 shows images of the aluminum drop on the surface of T7F3PM30 specimen at 960°C during the wettability test. From these images, the contact angles were measured as a function of time. The first image taken as the temperature reached 960°C (t=0) shows that the liquid Al drop was almost spherical. The contact angle between liquid aluminum and the specimen at this moment was 169°. After a while, the contact angle started to decrease. After 60 min the contact angle was 96° and only 14° after 175 min. After 185 min, liquid aluminum was completely spread over the surface which indicates that wetting occurs quite rapidly on this specimen and it has good wettability for liquid aluminum.

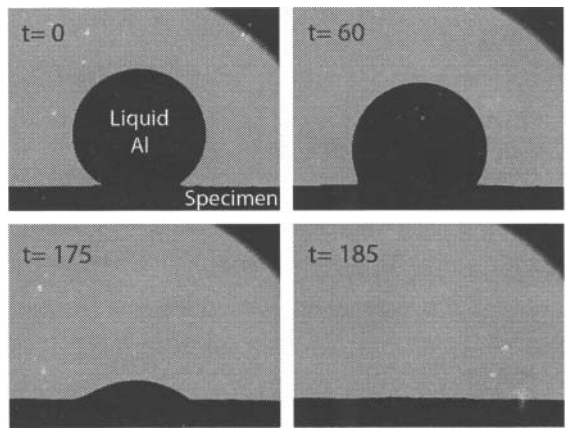

Figure 11- Behavior of liquid Al drop over T7F3PM30 specimen (TiB_2+7%Ti+3%Fe) during the wettability test at different time. (The time from beginning of test are reported in minutes)

The stability and reactivity of T7F3PM30 specimen in liquid aluminum have also been investigated. The specimen keeps its integrity after being exposed to liquid aluminum during 24h. Detailed results of these experiments will be published in an upcoming report.

Conclusions

TiB_2-based composites with 10% of Ti and Fe additives were consolidated using pressureless sintering. Specimens with 7%Ti+3%Fe additives showed better densification due to the formation of liquid phase during sintering. Best results were obtained for a sintering temperature of 1650°C. Pre-alloying of Fe and Ti before addition to TiB_2 powder significantly improved the densification. The milling time has also a marked influence on densification and on the properties of the sintered TiB_2 specimens. A maximum relative bulk density of 91% and maximum bending strength of 300 MPa were achieved with specimens milled for 30 min and sintered at 1650°C for 1h. The micrographs of specimens milled for 30 min reveal a uniform crack free microstructure with an even distribution of pores while those milled for longer times show the presence of numerous cracks in the specimens. The sintered specimens showed some resistance in liquid aluminum although more tests are needed. The resistance of specimens against aluminum infiltration and erosion are under investigation.

Acknowledgement

The authors wish to acknowledge the kind collaboration of the technicians of the Dept. Mining, Metallurgical and Materials Engineering of Laval University and of Sylvio Savoie from Hydro-Quebec. The financial support of this project was provided by Hydro Quebec and the Natural Sciences and Engineering Research Council of Canada (NSERC). The research project was also partially financed by the "Fonds Québécois de la Recherche

sur la Nature et les Technologies (FQRNT)" via the Aluminum Research Centre – REGAL.

References

[1] J.E. Hatch, Aluminum : properties and physical metallurgy, American Society for Metals, Metals Park, Ohio, 1984.
[2] F. Habashi, Extractive metallurgy of aluminum, in: G.E. Totten, D.S. Mackenzie (Eds.) Handbook of aluminum, CRC Press, 2003, pp. 1-46.
[3] M. Sørlie, H.A. Øye, Inert and wettable cathodes, in: Cathodes in aluminium electrolysis, Aluminium-Verlag, Düsseldorf, FRG, 1994, pp. 66-70.
[4] D.W. Richerson, Aluminum industry, in: D.W. Freitag, D.W. Richerson (Eds.) Opportunities for advanced ceramics to meet the needs of the industries of the future, US Office of Energy, 1998
[5] R. Telle, L.S. Sigl, K. Takagi, Boride-based hard materials, in: R. Riedel (Ed.) Handbook of ceramic hard materials, Wiley-VCH, Weinheim; Germany, 2000, pp. 802-945.
[6] R.A. Cutler, Engineering properties of borides, in: S.J. Schneider (Ed.) Engineering Materials Handbook, Ceramic and Glasses, ASM International, Metals Park, OH, USA, 1991, pp. 787–803.
[7] R.G. Munro, Material properties of titanium diboride, J. Res. Natl. Inst. Stan., 105 (2000) 709-720.
[8] H. Zhang, V. Nora, J.A. Sekhar, Materials used in Hall-Héroult cell for aluminium production, TMS, 1994.
[9] K. Billehaug, H.A. Oye, Inert cathodes for aluminum electrolysis in Hall - Heroult cells. Pt. I, Aluminum, 56 (1980) 642-648.
[10] C.J. McMinn, Review of RHM cathode development, in, Publ by Minerals, Metals & Materials Soc (TMS), San Diego, CA, USA, 1991, pp. 419-425.
[11] M.S. Jensen, M. Pezzotta, Z.L. Zhang, M.A. Einarsrud, T. Grande, Degradation of TiB_2 ceramics in liquid aluminum, Journal of the European Ceramic Society, 28 (2008) 3155-3164.
[12] M.S. Jensen, M.-A. Einarsrud, T. Grande, Preferential grain orientation in hot pressed TiB_2, J. Am. Ceram. Soc., 90 (2007) 1339-1341.
[13] T. Graziani, A. Bellosi, D.D. Fabbriche, Effects of some iron-group metals on densification and characteristics of TiB_2, Int. J. Refract. Met. Hard Mater., 11 (1992) 105-112.
[14] S. Torizuka, K. Sato, H. Nishio, T. Kishi, Effect of SiC on interfacial reaction and sintering mechanism of TiB_2, J. Am. Ceram. Soc., 78 (1995) 1606-1610.
[15] A. Petukhov, I. Khobta, A. Ragulya, A. Derevyanko, A. Raichenko, L. Isaeva, A. Koval'chenko, Reactive electric-discharge sintering of TiN-TiB_2, Powder Metall. Met. Ceram., 46 (2007) 525-532.
[16] S. Baik, P.F. Becher, Effect of oxygen contamination on densification of TiB_2, J. Am. Ceram. Soc., 70 (1987) 527-530.
[17] M.G. Barandika, J.J. Echeberría, J.M. Sánchez, F. Castro, Consolidation, microstructure, and mechanical properties of a TiB_2-Ni_3Al composite, Mater. Res. Bull., 34 (1999) 53-61.
[18] W.D. Kingery, H.K. Bowen, D.R. Uhlmann, Grain growth, sintering, and vitrification, in: Introduction to ceramics, Wiley, New York, 1976, pp. 448-515.
[19] P.S. Mohanty, J.E. Gruzleski, Mechanism of grain refinement in aluminum, Acta Metallurgica et Materialia, 43 (1995) 2001-2012.
[20] T.E. Quested, Understanding mechanisms of grain refinement of aluminium alloys by inoculation, Materials Science & Technology, 20 (2004) 1357.
[21] H. Okamoto, Fe-Ti (iron-titanium), Journal of Phase Equilibria, 17 (1996) 369-369.
[22] V.N. Eremenko, Y.V. Niadich, I.A. Lavrinenko, Capillary phenomena and wettability in liquid phase sintering process, in: Liquid phase sintering, Plenum Publishing Corporation, 1970, pp. 16-21.
[23] L. Ottavi, C. Saint-Jours, N. Valignant, C.H. Allibert, Phase equilibria and solidification of Fe-Ti-B alloys in the region close to Fe-TiB_2, Zeitschrift für Metallkunde, 83 (1992).
[24] V. Raghvan, B-Fe-Ti (Boron-Iron-Titanium), Journal of Phase Equilibria, 24 (2003) 455-456.
[25] T.H. Jungling, R. Oberacker, F. Thummler, L.S. Sigi, K.A. Schmetz, Pressureless sintering of TiB_2-Fe-materials, Powder Metall. Int., 23 (1991) 296-300.
[26] M. Palm, G. Inden, N. Thomas, The Fe-Al-Ti system, Journal of Phase Equilibria, 16 (1995) 209-222.
[27] ASTM_Standard, C1161-02c Standard test method for flexural strength of advanced ceramics at ambient temperature, in, ASTM International, West Conshohocken, PA, 2002.
[28] H. Baker, S.D. Henry, H. Okamoto, M.P.O.H.A.P.D.a.C. Asm International, ASM handbook. Vol. 3 : Alloy phase diagrams, ASM International, Materials Park, OH, 1992.
[29] R.M. German, Liquid-phase sintering, in: Sintering theory and practice, John Wiley & Sons, Ltd., 1996, pp. 225-313.